Biomedicine & Pharmacotherapy 77 (2016) 182–190

Available online at
ScienceDirect
www.sciencedirect.com

Elsevier Masson France
EM|consulte
www.em-consulte.com/en

Original article

Preparation and in vitro evaluation of 5-flourouracil loaded magnetite–zeolite nanocomposite (5-FU-MZNC) for cancer drug delivery applications

Tuğba Sağir[a], Merve Huysal[b], Zehra Durmus[c], Belma Zengin Kurt[d], Mehmet Senel[b,*], Sevim Isık[a,*]

[a] Department of Biology, Faculty of Arts and Sciences, Fatih University, B.Cekmece, Istanbul 34500, Turkey
[b] Institute of Biomedical Engineering, Fatih University, B.Cekmece, Istanbul 34500, Turkey
[c] Department of Pharmaceutical Biotechnology, Faculty of Pharmacy, Bezmialem Vakıf University, Fatih, 34093 Istanbul, Turkey
[d] Department of Pharmaceutical Chemistry, Faculty of Pharmacy, Bezmialem Vakıf University, Fatih, 34093 Istanbul, Turkey

ARTICLE INFO

Article history:
Received 22 October 2015
Received in revised form 16 December 2015
Accepted 21 December 2015

Keywords:
Nanoparticle
Zeolite
Magnetite
5-Flourouracil
In vitro study
Cancer

ABSTRACT

In this work, super paramagnetic magnetite nanoparticles were synthesized onto/into zeolite, then loaded with anti-cancer drug 5-fluorouracil (5-FU). The physical properties of the prepared nanocomposite and drug loaded nanocomposite were characterized using different techniques. The drug loading and releasing behavior of the magnetic nanocarrier was investigated and the drug-loaded nanoparticles exhibited a sustained release of drug without any burst release phenomenon. Furthermore, 5-FU loaded MZNC were evaluated for its biological characteristics. The functional 5-FU-MZNC has been triggered intra-cellular release of the cancer therapeutic agent 5-fluorouracil (5-FU). Cytotoxic effects of 5-FU loaded MZNC on human gastric carcinoma (AGS) cells were determined by real time cell analysis and colorimetric WST-1 cell viability assay. Apoptosis of cells was further investigated by Annexin-V staining which indicates the loss of cell membrane integrity. According to our results, 5-FU-MZNC showed a concentration-dependent cell proliferation inhibitory function against AGS cells. Morphologic and apoptotic images were consistent with the cytotoxicity results. In conclusion, 5-FU loaded MZNC efficiently inhibit the proliferation of AGS cells *in vitro* through apoptotic mechanisms, and may be a beneficial agent against cancer, however further animal study is still required.

1. Introduction

Nanomaterials can be used in many areas due to their electrical, optical, magnetic, and catalytic properties [1]. When nanomaterials turn into the hybrid material can be used in very different areas including protein/DNA bio-separation, disease diagnostics, cancer therapy, and drug and gene delivery [2–5].

Among all fields, cancer therapy is undoubtedly the most studied area. Cancer is a kind of complex disease which occurs mainly due to genetic or environmental factors. It is difficult to control growth without cell death. Cancer causes to a solid mass of cells known as a tumor or a liquid cancer [6]. Cancer is the second most common cause of death in Europe and North America [7]. Generally cancer patients are treated with traditional therapies such as surgery, chemotherapy, and radiotherapy. Chemotherapy is a type of systemic therapy affecting the whole body, uses medicines to control, slow or cure the cancer [8]. Chemotherapeutic drugs have a low specificity for the targeted tumor because they are dispersed overall the body [9], so toxic agents cause a serious risk to healthy tissues beside cancer cells.

Anticancer drugs are chemicals that are used for the treatment of cancer. Anticancer drugs can be divided into different categories according to their mechanism of action, such as alkylating agents, anti-metabolites, antitumor antibiotics and topoisomerase inhibitors, hormones and hormone antagonists, herbal remedies and other medications [10]. Cyclophosphamide, doxorubicin, docetaxel, methotrexate and fluorouracil are chemotherapeutic agents. They can be used alone or combination with other agents [11]. In a number of studies in recent years, chemotherapeutic nanoparticles include 5-fluorouracil which is a typical pyrimidine analogue [12–14]. It is used as cytotoxic agent in cancers of the gastrointestinal tract, breast tumors, and skin cancers [15].

* Corresponding authors. Fax: +90 2128663402.
E-mail addresses: msenel@fatih.edu.tr (M. Senel), isiksevim@fatih.edu.tr (S. Isık)

http://dx.doi.org/10.1016/j.biopha.2015.12.025
0753-3322/

Chemotherapy drugs also have some side effects for instance short blood half-life, elimination by the immune system and nonspecific targeting. In order to eliminate these side effects nanocarriers can be used in drug delivery systems as drug carriers [16]. Existing methods of cancer treatment are improved using nanocarriers. They reduce side effects of cancer drugs [9,18]. Nanocarriers can be composed of both organic and inorganic materials such as polymers, lipids (liposomes, nanoemulsions, and solid-lipid nanoparticles) self-assembling amphiphilic molecules, dendrimers, metals, and inorganic semiconductor nanocrystals (quantum dots) [19]. Living organisms are composed of cells with a diameter of around 10 μm. Uses of nanoparticles allow the observation of the functioning of the cells [1]. Nanoparticles have permeability and retention effect thus lead to leaky tumor vasculatures for better drug accumulation at the tumor sites [17]. With these advantages, nanoparticles gain importance to replace traditional chemotherapy.

Among nanocarriers, conventional magnetic material, Fe_3O_4 nanomaterials have been used in many fields such as lithium-ion batteries, wastewater treatment, magnetic resonance contrast media, therapeutic agents in cancer treatment and drug delivery. They have unique electric and magnetic properties. Especially superparamagnetic iron-oxide nanocomposites (SPIONs) are seen as a glimmer of hope for the cancer treatment because they have superparamagnetic behavior as well as surface-modification properties [20]. When they are used in biomedical applications they must have certain requirements. For instance in *in vivo* applications, encapsulation of magnetic nanoparticles in a biocompatible polymer have to be performed. Otherwise the original structure can change, large aggregates can form, and biodegradation can occur when interacted with biological systems. Thanks to the coating, drugs can bind [21].

Zeolites are a type of aluminosilicate crystal that can occur as natural or can be produced synthetically [22]. AlO_4 and SiO_4 tetrahedrons form nano size zeolite particles. Zeolites have microporous structure with cages and channels running through them. This architecture makes it as desirable candidates for treatment pollutants, sensing materials, and medical diagnostics [23]. They have somesignificant features such as small size, diverse frameworks, abundant accessible ion-exchanged sites, capacity for ionic exchange and high chemical, thermal, mechanical and radiation stability [24,22]. Especially advantage of these constructions, drug molecules can diffuse out of the channels by slow degrees so the rate of release is under control [25]. In a recent study, Vilaça et al. used two different zeolite types as drug carrier. They measued the drug release kinetics and found that 80-90% of the drug was released in the first 10 min [26].

In this study the anticancer drug 5-fluorouracil (5-FU) was encapsulated into magnetite–zeolite nanocomposite particles. The purpose of this work is to investigate the shapes of the particles, their size, drug loading and releasing capacity and biological activities in gastric cancer cell line AGS. Various structural (FT-IR SEM, XRD, TG) and the magnetization (VSM) characterizations were performed.

2. Experimental

2.1. Materials

Ferric chloride ($FeCl_3{\cdot}6H_2O$), ferrous chloride ($FeCl_2{\cdot}4H_2O$), ammonia water (NH_4OH), sodium hydroxide, 5-flourouracil and zeolite4A (molecular sieve ~350 mesh) were purchased from Sigma–Aldrich (St. Louis, MO, USA). All chemicals were of analytical grade and were used without further purification. Deionized milli-Q water was bubbled with high-purity nitrogen for 30 min before use.

2.2. Structural and physical characterization of samples

Structural and morphological features and thermal properties of the samples were investigated by Fourier transform infrared spectroscopy (FT-IR), X-ray diffractometry (XRD), scanning electron microscopy (SEM) and thermo gravimetric analysis (TGA). The crystallite size and phase structures of the samples were determined from the XRD patterns (Rigaku Smart Lab, Cu-Kα radiation). Fourier transform infrared (FT-IR) spectra of samples were recorded in transmission mode with a Bruker Alpha ATR spectrometer, in the wave number range of 400–4000 cm^{-1}. Magnetic properties of the samples were characterized by using a vibrating sample magnetometer (VSM, LDJ Electronics Inc., Model 9600) in an applied field of 15 kOe at room temperature. The morphological features of samples were investigated by a field emission SEM (FE-SEM, FEI Quanta FEG 450) operated at 30 kV. Powder samples were directly imaged in the electron microscope after a proper sample preparation of sputter-coated with gold.

2.3. Synthesis of magnetic zeolite nano composite

A mixed solution of ferrous and ferric ions in the molar ratio 1:2 was prepared by dissolving in 100 ml distilled water under vigorous stirring. Then a solution of concentrated NaOH was added to precipitate the iron oxides till the pH was raised to ~11 at which a black suspension was formed. The magnetite (Fe_3O_4) was directly prepared by precipitating iron salts under dropping NaOH, whereas for the nanocomposite sample, the zeolite 4A was added to the iron salts mixture prior to the reaction with NaOH. The amount of zeolite 4A was adjusted in order to obtain the following zeolite 4A/Fe_3O_4 weight ratios 1:1. This suspension was then refluxed at 90 °C for 12 h, under vigorous stirring and N_2 gas. Magnetic precipitates (MZNC) were separated from the supernatant solution by magnetic decantation, washed with distilled water three times and kept on a vacuum oven.

2.4. Drug loading and release procedure

The magnetite–zeolite nanocomposites (MZNC) were loaded with 5-FU by incubating 1 mg powder in 1 ml of 5-FU solutions with different concentrations and they were incubated for 24 h under vigorous mechanical stirring. The 5-FU-loaded mixtures (5-FU-MZNC) were centrifuged and the supernatant solutions were collected. The residual drug content was determined at a wavelength of 266 nm by ultraviolet visible spectroscopy using supernatant solutions to calculate the drug loading capacity of magnetite–zeolite nanocomposites.

For drug release experiments, the 5-FU-MZNC solutions were incubated in PBS at pH 5 and 7.4 for different periods of time. 5-FU released from magnetite–zeolite was collected by centrifugation at 14,800 rpm for 10 min. The amounts of released 5-FU in the supernatant solutions were determined by means of ultraviolet visible spectroscopy.

2.5. Cell culture

AGS cells were cultured in DMEM (Dulbecco's Modified Eagle Medium from GIBCO) medium containing 10% (v/v) fetal bovine serum (FBS), 1% penicillin-streptomycin, in a humidified atmosphere of 95% air and 5% CO_2 at 37 °C. Cells were subcultured twice a week for continuous culture.

2.6. Microscopic observation

After 24 h incubation with different concentrations (50, 100 and 200 μg/ml) of MZNC-5FU, detachment of the cells and

morphological changes were observed under inverted microscope (Nikon Eclipse TS100 inverted microscope). 20-fold magnification of the objective lens being used. The pictures were taken with a camera (Nikon).

2.7. Real time cell analysis

AGS cells were seeded at a density of 1×10^4 cells/well into E-plate that was used to generate dynamic real-time data with measuring electrical impedance across gold electrodes at the bottom of the plate. After 24 h, 5-FU-MZNC was prepared at concentrations of 200, 100, 50, 25, 10, 1 μg/ml and applied to the E-plate. The results were followed at real time during 63 h by the xCelligence system.

2.8. Cell proliferation assay, WST-1

The cytotoxicity of MZNC and 5-FU-MZNC on AGS cells was tested using the WST-1 cell proliferation assay kit (ROCHE). Cells were seeded at a density of 1×10^4 cells/well and incubated overnight in 96-well plate in 100 μl culture medium and then treated with molecules at 200, 100, 50, 25, 10, 1 μg/ml concentrations. After 24 h, 10 μl of WST-1 reagent was added to each well and the cells were incubated with the reagent for 4 h at 37 °C. The amounts of formazan in the wells were read on a microplate reader at 450 nm.

2.9. Annexin-V apoptosis assay

Cells were seeded into 96-well plate at 1.10^4/well and incubated overnight. The medium was replaced with fresh one containing the 50, 100 and 200 μg/ml concentrations of 5-FU-MZNC. After 24 h, Annexin-V-Alexa 568 (ROCHE) test was applied to the 96 well plate according to manufacturer's instructions. Afterwards, cells were observed under fluorescent microscope.

2.10. Statistical analysis

SPSS 18 programme was used to analyze the data. Data were evaluated by one way ANOVA. A $p < 0.05$ level was taken as significant.

3. Results and discussion

3.1. FTIR analysis

The FT-IR spectra of magnetite, zeolite 4A, MZNC, 5-FU and 5-FU-MZNC samples are recorded between 4000 and 400 cm^{-1}. The presence of the magnetite nanoparticles is evidenced by the strong absorption bands υ_1, observed at 600 cm^{-1} (red color) corresponds to intrinsic stretching vibrations of the metal at tetrahedral site (Fe_{tetra}–O), for naked magnetite but metal-oxygen band, υ_2, octahedral-metal stretching (Fe_{octa}–O) disappeared or overlapped for this sample although observed at 445 cm^{-1}, for MZNC sample. The bands at 456, 547 and 970 cm^{-1} are, respectively, related to the vibration of Si–O or Al–O bending, double ring and MeO_4 asymmetric stretch (Me = Si or Al). The band at 3000–3600 cm^{-1} represent inter and intermolecular hydrogen bonding. An absorption peak in the region of 3374 cm^{-1} corresponds to terminal silanol groups on the external surface of the zeolite crystals. A broad band between the 3000 and 3500 cm^{-1}, is attributed to NH stretching vibrations in the spectrum of 5-FU. The characteristic peak at 1736 cm^{-1} in the FT-IR spectrum of pure 5-FU is the vibration of C=O group. Also C—N streching at 1642 cm^{-1}, C—N vibration (in plane) at 1244 cm^{-1}, C-O vibration at 1186 cm^{-1} can be seen in the spectrumof 5-FU. When the 5-FU was incorporated into the MZNCs many characteristic peak in the FT-IR disappears because of the strong interaction between 5-FU and zeolite 4A. For example, after being incorporated into the zeolite NPs the characteristic absorbance peak of 5-FU at 1633 cm^{-1}, which corresponding to the C=O vibration, shifted to 1642 cm^{-1} and overlapped with the amino group of NPs. The FT-IR spectra results reveal that 5-FU is successfully encapsulated into the zeolite NPs [27] (Fig. 1).

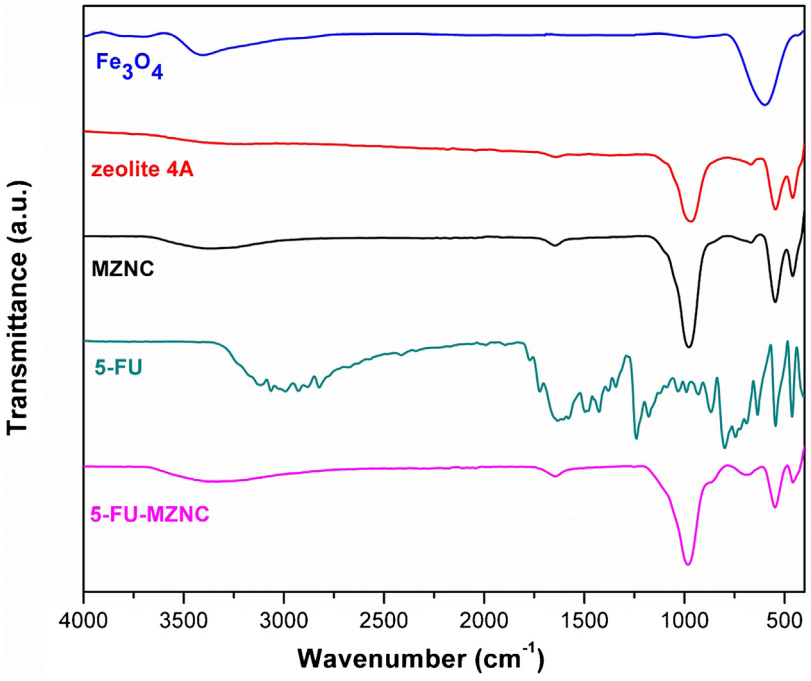

Fig. 1. FTIR spectra of Fe_3O_4, zeolite 4A, MZNC, 5-FU and 5-FU-MZNC samples.

3.2. XRD analysis

Fig. 2 shows the powder X-ray diffraction patterns of zeolite 4A, MZNC and Fe_3O_4 samples. The diffraction pattern for zeolite 4A, shown in Fig. 2, is similar to what has been reported in the literature [28,29] including crystalline aluminosilicate charactristic peaks as at $2\theta = 34.1$, 27.04, 29.88, 23.92, 16.04, 12.34, and 10.04 indicated that the microporous structure of zeolite. As clearly seen, XRD patterns of magnetite–zeolite nanocomposite samples which are essentially similar to diffraction of zeolite 4A that shown in Fig. 2. No additional Bragg reflections to indicate the existence of any additional crystalline phase or an overlapping broad diffraction pattern characteristic of an amorphous phase, have been observed for magnetite-zeolite composite samples [30]. In the XRD pattern of the MZNC sample the relative line intensity and line position related to zeolite 4A remained unchanged, indicating that during composite preparation, the crystal structure of zeolite 4A was stable. The diffraction line of iron oxide was observed at 2θ of 35.5 [27].

3.3. SEM analysis

SEM micrographs of Fe_3O_4, zeolite 4A and MZNC are shown in Fig. 3a–c, respectively. As it is clearly seen in Fig. 3a that SEM images of nano size magnetic Fe_3O_4 particles were smoothly sphere-shaped in appearance with approximately 30 nm in diameter as determined by MATLAB. Fine cubic morphology of zeolite 4A with homogenous morphology can be indicated in Fig. 3b. The particle size of Aldrich Zeolite 4A is around 2 μm with a broader size distribution. The external surface area of zeolite 4A was estimated from the particle size to be $\sim 4\ m^2/g$. In the composite structure, the presence magnetite onto zeolite surface was observed in Fig. 3. For composite sample reflux synthesis of magnetite has not altered the morphology and well-known crystalline structure of the both magnetite and zeolite 4A samples. It was found that the zeolite 4A amount into MZNC was about 50 wt%. The Al, Si and O ratios also confirmed the structure of zeolite 4A by EDS analysis in Fig. 3d. Presence of Cl atoms in the composition becomes from starter iron salts and Au atoms come from standard procedure of SEM sample preparation.

3.4. VSM analysis

The magnetic characterization of the samples was performed by M–H hysteresis measurements in a magnetic field range of ±15 kOe at room temperature. Fig. 4 shows that the magnetization increases with the applied field, whereas it does not reach to saturation even at maximum field of 15 kOe. In this case, the saturation magnetization (Ms) value can be calculated by the extrapolation of M–1/H curve for $1/H \rightarrow 0$. The Ms value of Fe_3O_4 sample was found to be 65 emu/g which was quite lower than that of bulk Fe_3O_4 (Ms = 92 emu/g) as expected [31].

This situation is expected phenoma for the hybrid nanoparticle systems and explained by the difference in spin ordering at the surface of the particles over that in the bulk resulting a magnetic core–shell structure. The weaker magnetization and lack of saturation are characteristic features of superparamagnetic particles having the smaller grain size than 20 nm [32]. Magnetization of these NPs can be described by the Langevin function and average particle size can be determined by theoretical fitting of this function to experimental (M–H) curves. By taking into account of the Ms value of Fe_3O_4 particles, 65 emu/g, the average particle size can be determined as 10.60 nm. The Ms value of MZNC sample was found to be 8.35 emu/g and the average particle size as 8.19 nm. It can be concluded that the entire surface spins of the magnetite particles were distorted presence the zeolite 4A in the medium and this effect drastically decreased the Ms value.

3.5. Drug loading-release studies

It can be seen clearly from Fig. 5A that the loading capacity of magnetite-zeolite nanocomposites increases with increase of the initial concentration of 5-FU. The saturated loading capacity can reach 0.668 mg mg^{-1} at the initial 5-FU concentration of 1 mg ml^{-1}. In view of the high loading capacity of 5-FU on magnetite–zeolite nanocomposites, it may be used as a promising drug carrier. To

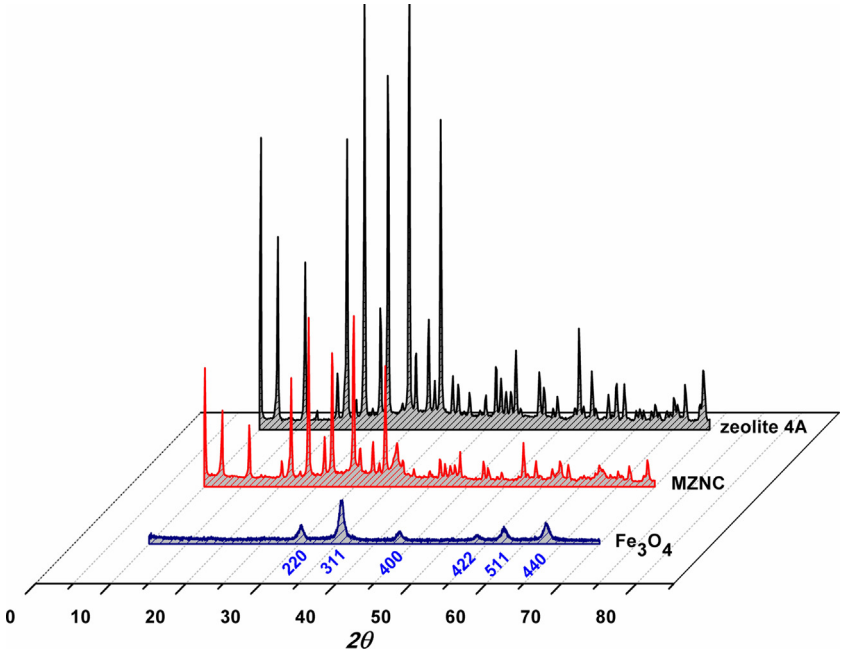

Fig. 2. XRD patterns of Fe_3O_4, zeolite 4A and MZNC samples.

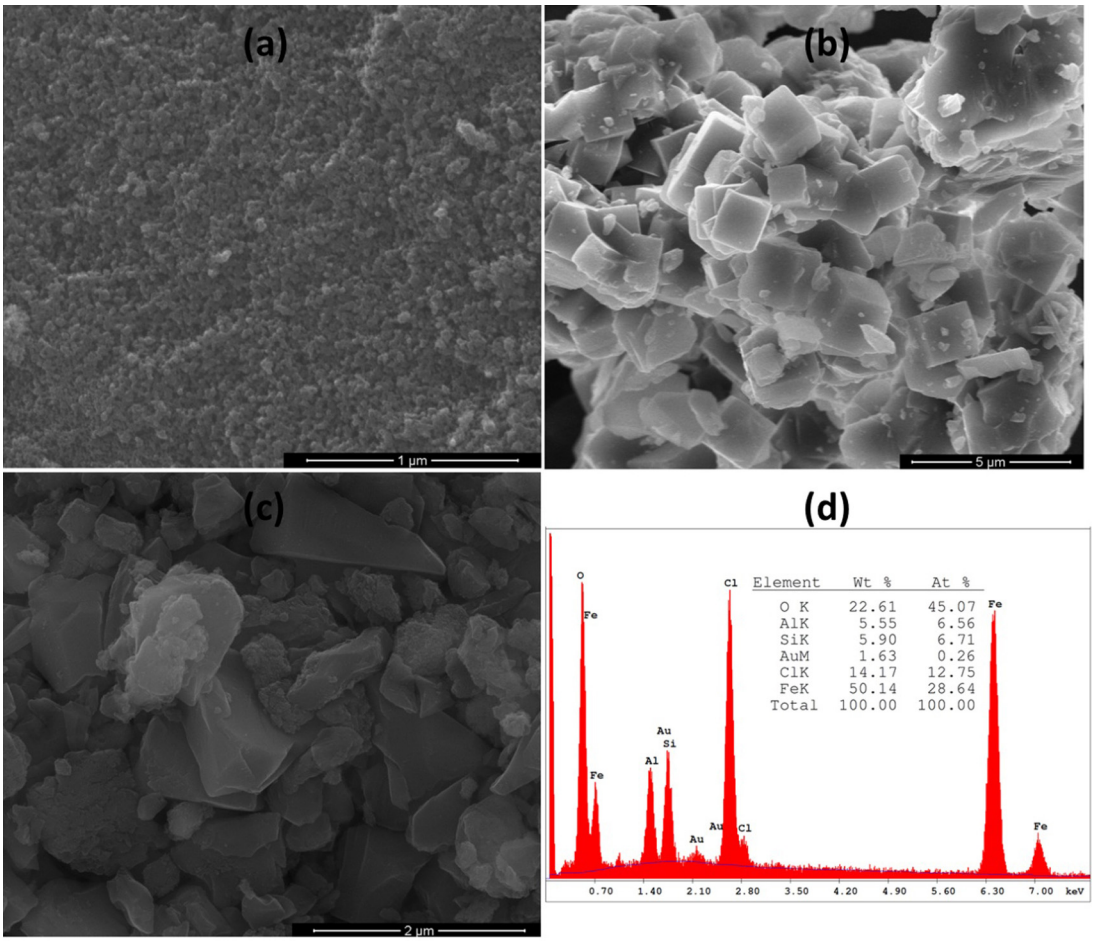

Fig. 3. SEM micrographs of (a) Fe_3O_4, (b) zeolite 4A (c) MZNC samples and (d) EDS analysis of MZNC samples.

further confirm the practicability of the obtained nanocomposites on controlled drug delivery, release kinetics of the loaded drug was investigated.

To understand the drug release behaviors of 5-FU loaded magnetite–zeolite (5-FU-MZNC) at neutral and acidic pH, magnetite–zeolite-5-FU nanocomposites were incubated in pH 7.4 and 5.0 PBS solutions at 37 °C in given Fig. 5B. The supernatants were measured by fluorescence spectroscopy after centrifugation at different time points. Within 360 min, about 90% of 5-FU was released from the nanocomposite at pH 5.0, while nearly 69% of 5-FU was released from pH 7.4 PBS. These results show that the release of 5-FU from magnetite-zeolite nanocomposites is pH-sensitive and when the pH decreased, accelerated release was observed. The reason for the increase of drug release in acidic medium can be changing of hydrogen bonding interaction between magnetite–zeolite and 5-FU. It can be expected that this sustained release of 5-FU will maintain a constant exposure of drug to the cancer cell resulting in enhanced anticancer effect and beneficial for drug delivery applications.

3.6. In vitro antitumor activity

Cell metabolism was analyzed real time for 63 h and how cells behave to different doses of 5-FU-MZNC molecule was observed. The optimal dose of 5-FU-MZNC was determined by xCelligence system. According to our real time cell analysis results, 5-FU-MZNC demonstrated a dose dependent cytotoxic effect on cells; 200, 100, 50, and 25 μg/ml 5-FU-MZNC molecules were more potent at reducing proliferation of AGS cells than 1 and 10 μg/ml in Fig. 6.

These results were confirmed by WST-1 assay by comparing MZNC and 5-FU-MZNC molecule at 200, 100, 50, 25, 10, 5, 1 μg/ml concentrations. It is clear that AGS cells gradually disappear or collapse with increasing the dosages of 5-FU-MZNC in the culture solution. The cell viability was carried out by taking into account the average of optical density whereas the statistic evaluation was based on the *t*-test (Paired Two Sample for Means). The difference in the cell viability of the samples, as reported to control cells, was statistically significant ($p < 0.05$) for 5-FU-MZNC. Although 5-FU-MZNC showed a significant effect at 25, 50, 100 and 200 μg/ml concentrations, MZNC itself did not demonstrate a significant effect at any concentration after 24 h on cell viability. 5-FU-MZNC molecule at 200 μg/ml caused 60% cell death. Since MZNC itself is not a toxic compound, it is a good choice for carrier material. MZNC becomes toxic if it is loaded with 5-FU and 5-FU loaded MZNC causes a toxic effect on AGS cells and lead them to apoptosis (Fig. 7).

Microscopically visible changes of cell morphology were investigated after 24 h of incubation with 5-FU-MZNC using AGS cells. The number of cells was reduced compared to control cells. Morphological changes revealed that after 24 h treatments with 5-FU-MZNC at 25, 50, and 100 μg/ml concentrations, cell proliferation was significantly inhibited. Cell blabbing and cytoplasmic degradation was observed under inverted microscopy. There was no change in the morphology of the untreated cells. They protected their right shapes (Fig. 8A).

To investigate the apoptotic effect of 5-FU-MZNC, AGS cells were treated with 50, 100 and 200 μg/ml 5-FU-MZNC, and after 24 h, Annexin-V assay was performed.

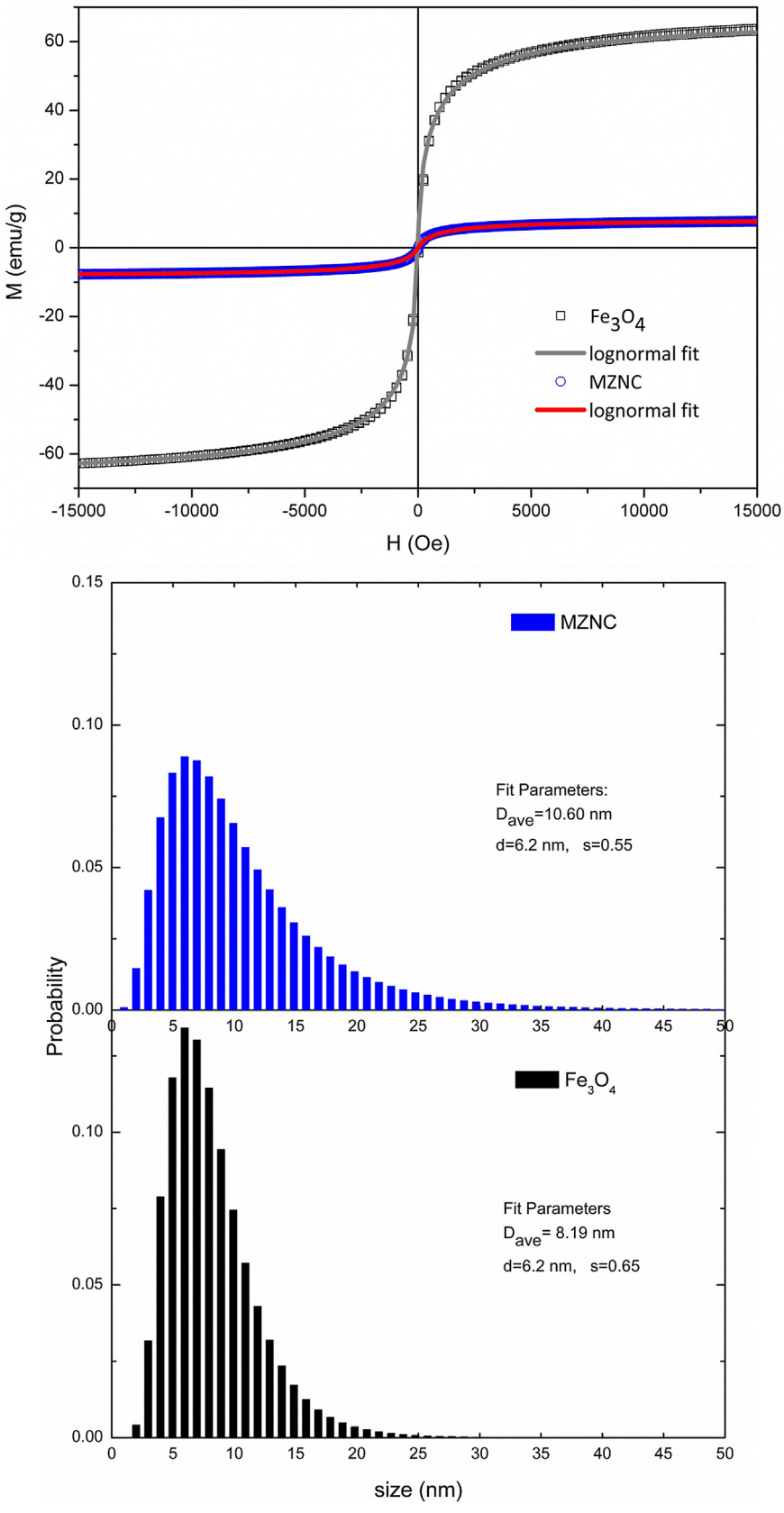

Fig. 4. *M–H* curves at room temperature and their log-normal size weighted Langevien fit of Fe_3O_4, and MZNC samples.

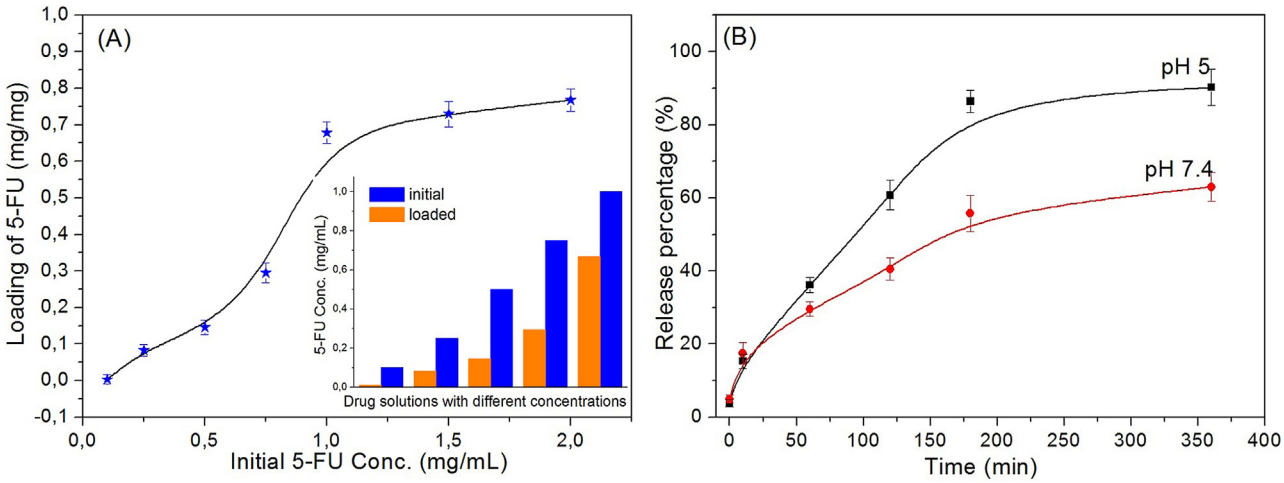

Fig. 5. (A) Drug loading capacity of MZNC at different initial 5-FU concentrations. (B) A plot of release of 5-FU from the MZNC in buffers at pH 5.0 and 7.4 at different time points.

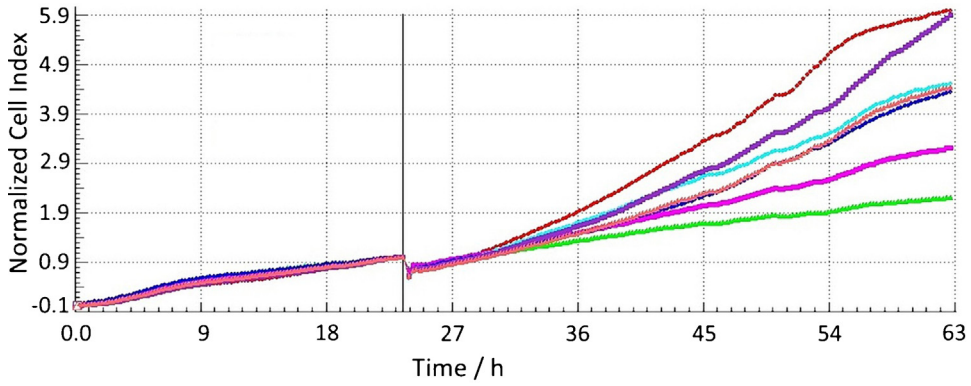

Fig. 6. Real time cell analysis of 5-FU-MZNC treated AGS cells. Cells were treated with 5-FU-MZNC at 200, 100, 50, 25, 10, 1 μg/ml concentrations. Real time cell analysis results of 5-FU-MZNC demonstrated a dose dependent cytotoxic effect on cells; 200, 100, 50, and 25 μg/ml 5-FU-MZNC molecules were more potent at reducing proliferation of AGS cells than 1 and 10 μg/ml. Experiments were performed in triplicates for all 5-FU-MZNC concentrations.

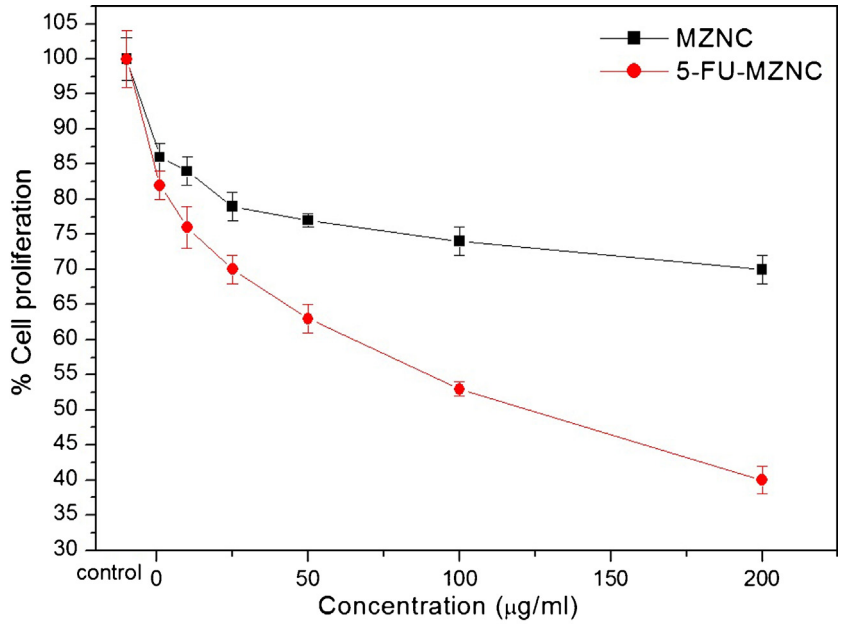

Fig. 7. Cell viability assay of MZNC and 5-FU-MZNC treated AGS cells. 5-FU-MZNC showed a significant effect at 25, 50, 100 and 200 μg/ml concentrations, on the other hand, MZNC itself did not demonstrate a significant effect at any concentration after 24 h on cell viability. The difference in the cell viability of the samples, as reported to untreated cells, was statistically significant ($p < 0{,}05$) for 5-FU-MZNC. Experiments were performed in triplicates for all MZNC and 5-FU-MZNC concentrations.

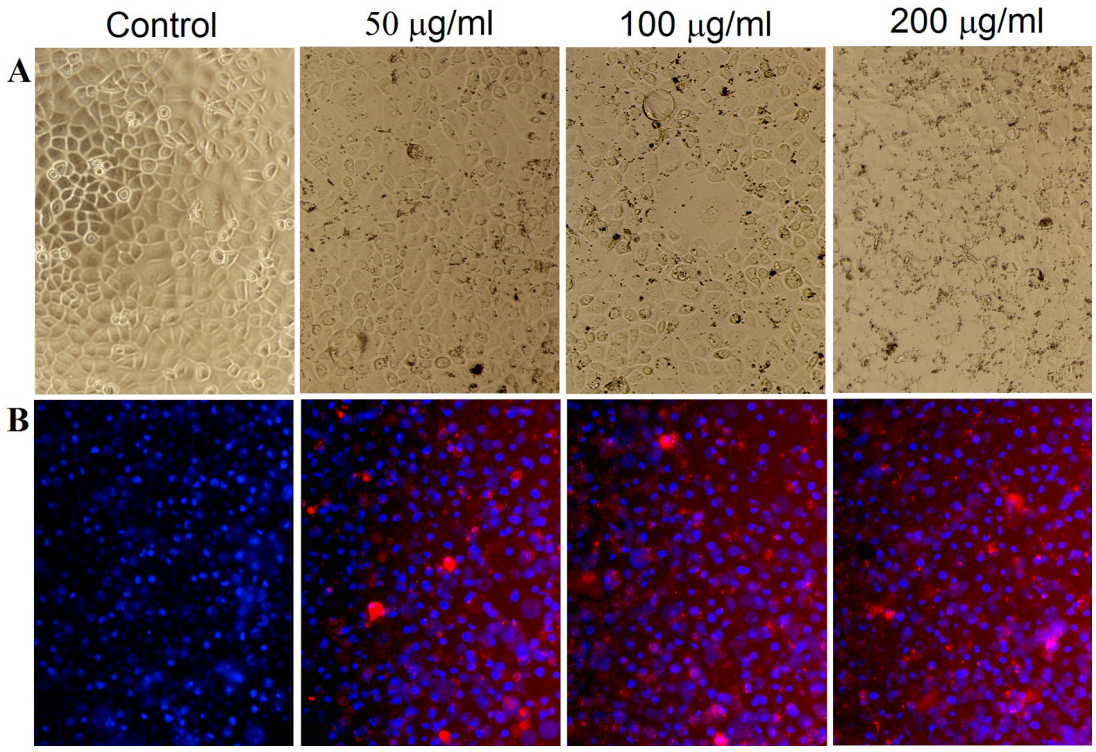

Fig. 8. Morphological and apoptotic changes. AGS cells were treated with 0, 50, 100, and 200 μg/ml concentrations of 5-FU-MZNC. Morphological changes revealed that after 24 h treatments with 5-FU-MZNC at 25, 50, and 100 μg/ml concentrations, cell proliferation was significantly inhibited and a significant increase in the number of apoptotic cells was observed compared with untreated AGS cells. Experiments were performed in triplicates for all 5-FU-MZNC concentrations.

According to the results, as shown in Fig. 8B, the viable cells turned into apoptotic cells. A significant increase in the number of apoptotic cells was observed compared with untreated AGS cells. Also concentration dependent higher apoptotic cells were observed under fluorescent microscopy. These results are expected to direct the applications of zeolite-nanocomposites with different structures and functionalities in pharmaceutical and clinic science.

4. Conclusion

5-Fluorouracil was successfully loaded into magnetic zeolite nanocomposite yielding stable fluorescent hybrid nanoparticles with near-infrared optical properties. The biological assays confirmed the association of the 5-fluorouracil to the MZNC and their functionality in a cell-based assay system. The outcome of the current study is application a simple method for the preparation and characterization of 5-FU loaded superparamagnetic zeolite–magnetite nanocomposites which yielded a significant decrease in cell viability (200 μg/ml 5-FU-MZNC, 60% cell death) *in vitro*. Cell viability shows that vehiculization of the drug improves the cytotoxic effect in comparison with the one produced by the free 5-fluorouracil itself. The drug nanoparticles were nanosized and exhibited a controlled and sustained release of drug without any burst release phenomenon. 5-FU-MZNC could inhibit the proliferation of AGS cells and induce greater apoptosis to AGS cells line in comparison with the MZNC, which displayed time or concentration-dependent manner. Therefore, we expect that MZNC could be an effective carrier and also targeted to tumor site under the control of an external magnetic field for chemotherapeutic drug delivery and further *in vivo* studies are needed to be carried out to prove the therapeutic potential of the present tumor-specific delivery system.

Acknowledgement

The author is thankful to the Bezmialem Vakif University Research Project Foundation (Project no.: 9.2013/4) for financial support of this study.

References

[1] O. Salata, Applications of nanoparticles in biology and medicine, J. Nanobiotechnol. 2 (2004) 1–6.
[2] M. De, P.S. Ghosh, V.M. Rotello, Applications of nanoparticles in biology, Adv. Mater. 20 (2008) 4225–4241.
[3] G. Braun, S.J. Lee, M. Dante, T.Q. Nguyen, M. Moskovits, N. Reich, Surface enhanced Raman spectroscopy for DNA detection by nanoparticle assembly onto smooth metal films, J. Am. Chem. Soc. 129 (2007) 6378–6379.
[4] A.K. Gupta, M. Gupta, Synthesis and surface engineering of iron oxide nanoparticles for biomedical applications, Biomaterials 26 (2005) 3995–4021.
[5] N.L. Rosi, D.A. Giljohann, C.S. Thaxton, A.K. Lytton-Jean, M.S. Han, C.A. Mirkin, Oligonucleotide-modified gold nanoparticles for intracellular gene regulation, Science 312 (2006) 1027–1030.
[6] S. Nussbaumer, P. Bonnabry, J.L. Veuthey, S. Fleury-Souverain, Analysis of anticancer drugs: a review, Talanta 85 (2011) 2265–2289.
[7] Ajit S. Narang, Divyakant S. Desai, Anticancer drug development, Pharmaceutical Perspectives of Cancer Therapeutics, Springer Science +Business Media LLC, 2009, pp. 49–92.
[8] C.M. Jack Hu, S. Aryal, L. Zhang, Nanoparticle-assisted combination therapies for effective cancer treatment, Ther. Deliv. (2010) 323–334.
[9] K.R. Javed, M. Ahmad, S. Ali, M.Z. Butt, M. Nafees, A.R. Butt, M. Nadeem, A. Shahid, Comparison of doxorubicin anticancer drug loading on different metal oxide nanoparticles, Medicine 94 (2015) 617.
[10] T. Taşkın-Tok, S. Gowder, Anticancer drug—friend or foe, Pharmacol. Ther. (2014) 255–269.
[11] H. Banu, D.K. Sethi, A. Edgar, A. Sheriff, N. Rayees, N. Renuka, S.M. Faheem, K. Premkumar, G. Vasanthakumar, Doxorubicin loaded polymeric gold nanoparticles targeted to human folate receptor upon laser photothermal therapy potentiates chemotherapy in breast cancer cell lines, J. Photochem. Photobiol. B 149 (2015) 116–128.
[12] R.C. Nagarwal, P.N. Singh, S. Kant, P. Maiti, J.K. Pandit, Chitosan nanoparticles of 5-fluorouracil for ophthalmic delivery: characterization, in-vitro and in-vivo study, Chem. Pharm. Bull. 59 (2011) 272–278.

[13] Daniel B. Longley, D. Paul Harkin, Patrick G. Johnston, 5-Fluorouracil: mechanisms of action and clinical strategies, Nat. Rev. Cancer 3 (2003) 330–338.
[14] B. Pardini, R. Kumar, A. Naccarati, 5-Fluorouracil-based chemotherapy for colorectal cancer and MTHFR/MTRR genotypes, Br. J. Clin. Pharmacol. 72 (2011) 162–163.
[15] S. Nussbaumer, P. Bonnabry, J.L. Veuthey, S. Fleury-Souverain, Analysis of anticancerdrugs: a review, Talanta 85 (2011) 2265–2289.
[16] P. Yu, X.M. Xia, M. Wu, C. Cui, Y. Zhang, L. Liu, B. Wu, C.X. Wang, L.J. Zhang, X. Zhou, R.X. Zhuo, S.W. Huang, Folic acid-conjugated iron oxide porous nanorods loaded with doxorubicin for targeted drug delivery, Colloids Surf. B 120 (2014) 142–151.
[17] Y. Matsumura, H. Maeda, A new concept for macromolecular therapeutics in cancer chemotherapy: mechanism of tumoritropic accumulation of proteins and the antitumor agent smancs, Cancer Res. 46 (1986) 6387–6392.
[18] S. Kayal, R.V. Ramanujan, Anti-cancer drug loaded iron–gold core–shell nanoparticles (Fe@Au) for magnetic drug targeting, J. Nanosci. Nanotechnol. 10 (2010) 5527–5539.
[19] S. Ganta, H. Devalapally, A. Shahiwala, M. Amiji, A review of stimuli-responsive nano carriers for drug and gene delivery, J. Control. Release 126 (2008) 187–204.
[20] H. Shen, J. Chen, H. Dai, L. Wang, M. Hu, Q. Xia, NEw insights into the sorption and detoxification of chromium(VI) by tetraethylenepentamine functionalized nanosized magnetic polymer adsorbents: mechanism and pH effect, Ind. Eng. Chem. Res. 52 (2013) 12723–12732.
[21] A. Akbarzadeh, M. Samiei, S. Davaran, Magnetic nanoparticles: preparation, physical properties, and applications in biomedicine, Nanoscale Res. Lett. 7 (2012) 144.
[22] Y. Peña, W. Rondón, Linde type a zeolite and type Y faujasite as a solid-phase for lead, cadmium, nickel and cobalt preconcentration and determination using a flow injection system coupled to flame atomic absorption spectrometry, Am. J. Anal. Chem. 4 (2013) 387–397.
[23] P. Sharma, J. Yeo, D.K. Kim, C.H. Cho, Organic additive free synthesis of mesoporous naoncrystalline NaA zeolite using high concentration inorganic precursors, J. Mater. Chem. 22 (2012) 2838–2843.
[24] T. Kihara, Y. Zhang, Y. Hu, Q. Mao, Y. Tang, J. Miyake, Effect of composition, morphology and size of nanozeolite on its in vitro cytotoxicity, J. Biosci. Bioeng. 111 (2011) 725–730.
[25] M. Spanakis, N. Bouropoulos, D. Theodoropoulos, L. Sygellou, S. Ewart, A.M. Moschovi, A. Siokou, I. Niopas, K. Kachrimanis, V. Nikolakis, P.A. Cox, I.S. Vizirianakis, D.G. Fatouros, Controlled release of 5-fluorouracil from microporous zeolites, Nanomedicine 10 (2014) 197–205.
[26] N. Vilaça, R. Amorim, A.F. Machado, P. Parpot, M.F.R. Pereira, M. Sardo, J. Rocha, A.M. Fonseca, I.C. Neves, F. Baltazar, Potentiation of 5-fluorouracil encapsulated in zeolites as drugdelivery systems for in vitromodels of colorectalcarcinoma, Colloids Surf. B 112 (2013) 237–244.
[27] P. Li, Y. Wang, Z. Peng, M.F. She, L. Kong, Physichemical property and morphology of 5-fluorouracil loaded chitosan nanoparticles, 2010 International Conference on Nanoscience and Nanotechnology (ICONN) (2010) , doi:http://dx.doi.org/10.1109/ICONN.2010.6045203.
[28] D.W. Breck, Zeolite molecular sieves: structure, Chemistry and Use, Wiley, England, 1974, pp. p353.
[29] M.M.J. Treacy, J.B. Higgins, Collection of Simulated XRD Powder Patterns For Zeolites, 5th ed., Elsevier, 2007.
[30] S.K. Kulshreshtha, R. Vijayalakshmi, V. Sudarsan, H.G. Salunke, S.C. Bhargava, Iron oxide nanoparticles in NaA zeolite cages, Solid State Sci. 21 (2013) 44–50.
[31] D.H. Han, J.P. Wang, H.L. Luo, Crystallite size effect on saturation magnetization of fine ferromagnetic particles, J. Magn. Magn. Mater. 136 (1994) 176–182.
[32] J. Mürbe, A. Rechtenbach, J. Töpfer, Synthesis and physical characterization of magnetite nanoparticles for biomedical applications, Mater. Chem. Phys. 110 (2008) 426–443.